bioRxiv preprint doi: https://doi.org/10.1101/2022.05.15.491997; this version posted May 15, 2022. The copyright holder for this preprint (which was not certified by peer review) is the author/funder, who has granted bioRxiv a license to display the preprint in perpetuity. It is made available under aCC-BY-NC 4.0 International license.

Identifying the Neural Correlates of Balance Deficits in Traumatic Brain Injury using the Partial Least Squares Correlation (PLSC) analysis

Vikram Shenoy Handiru[1,2], Easter S. Suviseshamuthu[1,2], Soha Saleh[1,2], Guang H. Yue[1,2], Didier Allexandre[1,2]

[1]Center for Mobility and Rehabilitation Engineering Research, Kessler Foundation, New Jersey, USA. [2]Department of Physical Medicine and Rehabilitation, Rutgers University-New Jersey Medical School, Newark, USA.

Correspondence should be addressed to Vikram S. Handiru; vshenoy@kesslerfoundation.org

Abstract

Balance impairment or the loss of balance control is one of the most debilitating consequences of Traumatic Brain Injury (TBI). The levels of balance impairment may not be necessarily associated with the severity level of TBI, which makes it more difficult to do the correlational analysis of the balance impairment and its neural underpinnings. Therefore, we conducted a study where we collected the neurophysiological data (EEG and EMG) during a balance control task on a computerized posturography platform in a group of 17 TBIs and 15 age-matched healthy controls. Further, to distinguish balance-impaired TBIs (BI-TBI) from non-impaired TBIs (BN-TBI), we stratified the level of balance impairment using the Berg Balance Scale, a functional outcome measure widely used in both research and clinical settings. We computed the brain functional connectivity features between different cortical regions of interest using the imaginary part of coherence in different frequency bands. These features are then studied in a mean-centered Partial Least Squares Correlation analysis, which is a data-driven framework with the advantage of handling more features than the number of samples, thus making it suitable for a small-sample study. Based on the nonparametric significance testing using permutation and bootstrap procedure, we noticed that theta-band connectivity strength in the following ROIs significantly contributed to distinguishing balance impaired from non-impaired population: left middle frontal gyrus, right precuneus, right precentral gyrus, bilateral middle occipital gyrus, right middle temporal gyrus, left superior frontal gyrus, left post-central gyrus, right paracentral lobule. The knowledge of specific neural regions associated with balance impairment helps better understand neural mechanisms of TBI-associated balance dysfunction and may guide the development of novel therapeutic strategies, including targeted noninvasive brain stimulation. Our future studies will investigate the effects of balance platform training on sensorimotor connectivity.

bioRxiv preprint doi: https://doi.org/10.1101/2022.05.15.491997; this version posted May 15, 2022. The copyright holder for this preprint (which was not certified by peer review) is the author/funder, who has granted bioRxiv a license to display the preprint in perpetuity. It is made available under aCC-BY-NC 4.0 International license.

1. Introduction

Traumatic Brain Injury (TBI) is one of the leading causes of death and disability across the globe [1]. With the immediate consequences of long-term disability due to the injury, TBI patients are often at elevated risks of impaired motor functions such as loss of postural control [2]. While it is postulated that the postural imbalance could be attributed to the loss of sensorimotor integration after injury [3], the exact neurophysiological mechanisms are unknown [4].

With the advances in the current neuroimaging technologies such as high-density electroencephalography and functional Near-Infrared Spectroscopy (fNIRS), mobile imaging of body-brain behavior is possible. Although there are some studies evaluating balance-related brain functional connectivity changes in healthy individuals using fNIRS [5] and EEG [6], there are hardly any such studies in TBI populations. The current state-of-the-art in understanding neuroanatomy and neurophysiology is limited to the findings from structural imaging using Diffusion Tensor Imaging (DTI) [7,8] and resting-state functional Magnetic Resonance Imaging (rs-fMRI) [9]. This motivated us to fill the knowledge void of the underlying neural substrates of postural control in TBI. Identifying the neural markers of postural control can potentially guide us in developing novel therapeutic strategies to address the postural instability in TBI.

This brings us to some of the key research questions:

1. Why do some TBIs have more balance impairment than others?

2. Which brain regions and networks play a crucial role in balance control?

3. How does the TBI alters the modulation of motor-related functional networks during the postural control task?

4. Can we identify a diagnostic neural marker of balance deficits in TBI?

Addressing these questions requires stratifying the brain injury population into balance-impaired and balance non-impaired as not every TBI patient suffers from the same degree of postural instability. Moreover, the heterogeneity in the type of brain injury adds to the challenges of neural data processing. This motivates us to study the brain dynamics in balance-impaired as well as balance non-impaired populations in comparison with the healthy controls.

While it is widely accepted that the external sensory cues trigger the shift of attention away from the ongoing balance task-irrelevant cognitive activity towards the balance task-relevant cognitive activity during postural control [10], the interaction between different networks is not well understood. We hypothesize that a relatively complex task of postural control when faced with external perturbation cues, requires the involvement of multiple networks. Our research motivation is further fuelled by the paucity of literature on the interacting effects of different brain networks pertaining to anticipatory postural control. To this end, not only are we interested in studying the network-level mechanisms of postural control but also in exploring the individual connectivity features associated with the balance impairment in a hypothesis-driven approach by defining the regions of interest (ROI).

In a resting-state fMRI study focused on the functional connectivity alterations within- and between networks in the TBI population, it was observed that the Default Mode Network (DMN) showed reductions in within-network and also between-network connections with the Dorsal Attention Network (DAN) when compared to healthy controls [9]. The authors state that these pronounced disruptions in between-network connectivity in chronic TBI would have been missed if the integrity of only a single network was evaluated. Motivated by this idea, we want to further study how TBI affects the task-specific cognitive-motor related network during the postural control which has not been previously explored.

bioRxiv preprint doi: https://doi.org/10.1101/2022.05.15.491997; this version posted May 15, 2022. The copyright holder for this preprint (which was not certified by peer review) is the author/funder, who has granted bioRxiv a license to display the preprint in perpetuity. It is made available under aCC-BY-NC 4.0 International license.

Intuitively, some of the approaches that seem to address this question look at the correlation between the brain activity/functional networks in the brain and a quantifiable functional measure of balance deficits. To this end, Partial Least Squares (PLS)-based approach is a powerful and robust statistical method used to find a fundamental relationship between a large set of variables, which has been recently explored and useful in identifying the brain-behavior association. Using this approach, Churchill et al. [11] observed higher connectivity between the default-mode and sensorimotor network to be associated with sport-related concussion and balance symptom severity. Extending further in this direction, we are using this data-driven PLS method (Fig. 1) to extract neural markers of balance impairment in chronic TBI.

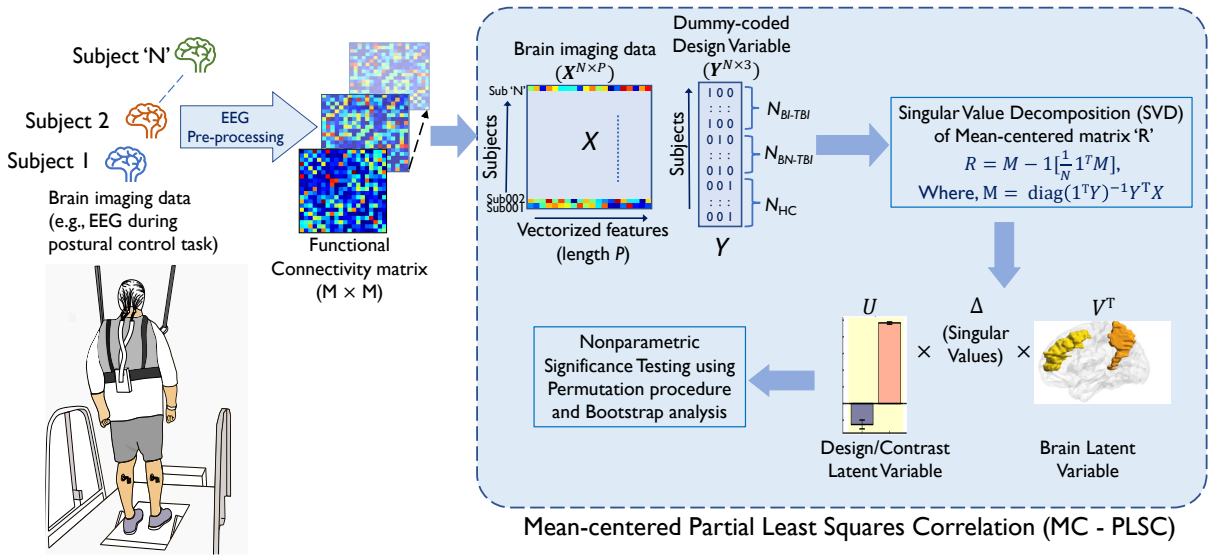

Figure 1: The mean-centered Partial Least Squares correlation (MC-PLSC) analysis framework begins with the vectorized functional connectivity features derived from preprocessed source-localized EEG. The mean-centered vectorized features for each subject as a row vector constitute a matrix (X) for N subjects. The product of the design matrix (Y) and brain imaging feature matrix (X) is then subjected to Singular Value Decomposition (SVD) which results in a set of mutually orthogonal latent variables (LVs). Left singular vector corresponds to the design/contrast LV (e.g., HC vs. TBI) whereas the right singular value corresponds to the brain LV which indicates the functional connectivity pattern associated with the contrast.

2 Methodology

2.1 Participant Characteristics

This study enrolled 18 individuals with a chronic Traumatic Brain Injury (TBI) and 18 Age-matched healthy controls (HC). Due to the highly noisy EEG data of some participants, we had to exclude the data from 1 TBI and 3 HC subjects, thus we present the data from 17 TBI and 15 HC in this paper. More information on the subject demographics including the inclusion and exclusion criteria for the study participants can be found in [12]. To identify a neural marker of balance deficit within the TBI population, we dichotomized the TBI group into balance-impaired (BI-TBI) vs. balance non-impaired TBI (BN-TBI) based on the threshold for Berg Balance Scale (BBS) score. A BBS threshold score of 49 (out of the maximum 56 points) was chosen to define balance impairment as it was shown to optimally identify individuals with balance deficits during ambulation in terms of needing a walking aid [13]. Using this stratification based on the BBS threshold, we

bioRxiv preprint doi: https://doi.org/10.1101/2022.05.15.491997; this version posted May 15, 2022. The copyright holder for this preprint (which was not certified by peer review) is the author/funder, who has granted bioRxiv a license to display the preprint in perpetuity. It is made available under aCC-BY-NC 4.0 International license.

Table 1: TBI Patient Demographics and Clinical Characteristics (N = 17)

Subj_ID	Group	Gender	Age	Height (cm)	Weight (kg)	COP (cm)	BBS	Severity
ABI001	BI-TBI	M	51	190.5	95.3	9.39	48	Severe
ABI002	BI-TBI	M	58	182.9	88	7.31	42	Severe
ABI003	BI-TBI	M	60	175.9	88.7	19.18	44	Severe
ABI004	BI-TBI	M	59	178.4	143.8	13.49	49	Severe
ABI005	BN-TBI	M	51	180.3	113.9	9.47	54	Mild
ABI006	BN-TBI	M	52	177.8	97.5	12.86	54	Severe
ABI007	BN-TBI	F	53	170.2	76.2	18.0	51	Mild
ABI008	BI-TBI	M	60	180.3	111.1	8.19	48	Mild
ABI009	BN-TBI	F	32	167.6	58.5	10.12	56	Mild
ABI010	BI-TBI	M	49	172.7	66.7	14.14	46	Mild
ABI012	BN-TBI	F	56	168.9	120.2	4.8	55	Mild
ABI013	BI-TBI	F	60	154.3	72.6	17.27	34	Moderate
ABI016	BN-TBI	M	56	182.9	86.2	7.32	56	Mild
ABI018	BI-TBI	M	35	182.9	68	15.33	44	Moderate/severe
ABI019	BN-TBI	M	23	177.8	63.5	7.44	55	Severe
ABI020	BN-TBI	M	50	187.96	102.1	9.17	55	Moderate/severe
ABI021	BN-TBI	M	23	182.88	89.4	14.54	52	Moderate/severe

obtained the subgroup sample of BN-TBI ($N = 9$) and BI-TBI ($N = 8$) (Fig. 2B). The patient demographics and clinical characteristics of TBI participants are presented in Table 1.

2.2 Data Acquisition and Pre-processing

We used multiple modalities to collect EEG and the posturography platform data during a balance perturbation task and MRI to obtain subject-specific anatomical data for EEG source localization.

(A) **MRI Data Acquisition:** The MRI data (T1-weighted MPRAGE scan) was acquired at the Rocco Ortenzio Neuroimaging Center (Kessler Foundation, NJ) using the Siemens Skyra 3T scanner (Erlangen, Germany) with the following specifications: 1-mm isotropic voxel resolution, TE=3 ms, TR=2300 ms, 1-mm thick 176 slices, Field of View (FOV) 256x256 mm2.

(B) **Posturography Data Acquisition:** The perturbation-related data was measured using the computerized dynamic posturography (CDP) platform (NeuroCom Balance Master, NeuroCom Intl, Clackamas OR). This computerized platform was pre-programmed to generate unpredictable sinusoidal perturbations at low amplitude (0.5 cm) or high amplitude (2 cm) in the anterior-posterior (or forward and backward) direction at 0.5Hz for 4s with a random intertrial interval between 4-8s. The posturography data were collected in 5 blocks where each block consisted of 20 trials randomly sorted among a 2 x 2 combination of High/Low amplitude and Forward/Backward perturbations. In this study, we mainly present the findings from a total of 29 trials of high amplitude backward perturbation, the most challenging condition with the highest range of body sway across subjects. The center of pressure (COP) time-series data from the balance platform was collected at 200 Hz, and offline low-pass filtered (10Hz), epoched, and mean-centered (zero-mean), and averaged across trials and conditions for each subject. The COP displacement was calculated as the trial average (in cm) of the cumulative distance traveled by the COP vector for the first 2s of the perturbation in the forward/backward direction.

(C) **EEG Data Acquisition**: The brain activities during the balance perturbation were noninvasively recorded using the 64-channel EEG system (ActiCAP BrainAmp standard, Brain Products®, Munich, Germany) at a sampling rate of 500 Hz. The EEG electrodes were positioned according to the extended

bioRxiv preprint doi: https://doi.org/10.1101/2022.05.15.491997; this version posted May 15, 2022. The copyright holder for this preprint (which was not certified by peer review) is the author/funder, who has granted bioRxiv a license to display the preprint in perpetuity. It is made available under aCC-BY-NC 4.0 International license.

10-10 montage with the electrodes FCz serving as the common reference and AFz the ground.

2.3 Data Processing

The recorded EEG was processed offline using EEGLAB and BrainStorm toolboxes. First, we preprocessed the raw continuous EEG by downsampling it into 250 Hz followed by band-pass filtering between 1Hz and 50Hz using a Butterworth filter (4th order) to ensure the frequency bands of interest are covered. The electrical line noise was removed using the Cleanline plugin for EEGLAB. Thereafter, the noisy bursts in the continuous EEG were corrected using Artifact Subspace Reconstruction. The burst detection criteria threshold (k in the ASR algorithm) was set at 20 based on the comprehensive evaluation by [14]. After applying the common-average referencing to the ASR-corrected data, we ran the Independent Component Analysis (ICA) (extended Infomax algorithm)[15]. The independent components resulting from ICA decomposition were then classified into one of the following labels ((1) Brain, (2) Muscle, (3) Eye, (4) Line noise, (5) Channel noise, (6) Heart or (7)'other') using a machine-learning tool ICLabel plugin within EEGLAB [16]. The dipole fitting was done using the DIPFIT tool in EEGLAB which can be used to assess whether the dipoles corresponding to the ICs are 'brain'-based or not.

We retained only those ICs that are classified as 'Brain' (posterior probability > 0.5) and the residual variance (relative to the scalp topography) of 20%. Upon selecting these ICs, the back-projected sensor-space EEG was used for EEG Source Localization.

2.4 EEG Source Localization (ESL)

Since the brain activity recorded at the scalp level gets attenuated due to the volume conduction effect (propagation of electric current flow through different layers of the brain and skull), it is advisable to estimate the cortical source activity [17]. To achieve this, we used the OpenMEEG tool [18] in the Brainstorm toolbox [19] to compute the forward head model wherein a realistic head model made of 4 layers (brain, inner skull, outer skull, and scalp surface) is reconstructed using individual T1 MRI scans and the 3D EEG electrode positions using Brainsight Neuronavigation System (Rogue Research, Montreal, Canada). The volume conduction effect is realized using the Boundary Element Model [20]. Once the forward model is obtained, we used sLORETA [21] algorithm as a distributed source model to solve the ill-posed inverse problem. Estimating the solution using sLORETA requires the computation of the noise covariance matrix in addition to the forward head model. Therefore, the noise covariance estimation was done using the 'baseline' EEG which is essentially the pre-perturbation period (-1s to 0s). Once we obtained the source-localized EEG, we parcellated the cortical surface into 66 anatomical regions using a surface-volume registration tool in BrainSuite software [22]. Thereafter, the key regions of interest for further analyses (functional connectivity estimation and the partial least squares analysis) were determined based on the literature and our preliminary study [12] in which we identified which cortical regions were significantly more activated during the perturbation compared to the baseline period. To avoid any bias concerning the hemispheric dominance, we included bilateral ROIs from the middle frontal gyrus, superior frontal gyrus, middle temporal gyrus, paracentral lobule, precentral gyrus, postcentral gyrus, precuneus, cingulate gyrus, superior parietal lobule, and middle occipital gyrus.

2.5 Functional Connectivity

The brain functional connectivity between two regions of interest was calculated for the time segments (0s-2s) corresponding to the perturbation task and baseline state using imaginary coherence (iCOH) [23]. Here, the time instant at which perturbation occurs is noted as $t = 0$s. The imaginary coherence is considered to be a robust estimate of phase synchronization between two time-series data. To ensure computational tractability, we measured the iCOH between the 'seed' voxels of different ROIs instead of every pair of voxels in an ROI. Mathematically, we denote the iCOH as the imaginary part of coherence i.e., $\mathrm{Im}(\underline{\mathbf{\Gamma}})$ with , where, $\underline{\mathbf{\Gamma}} \in \mathbb{C}^{U \times U \times V}$ is a three-way tensor, where U and V are the number of ROIs and frequency bins of interest, respectively. Since the iCOH values are computed for each frequency bin, we averaged the iCOH

bioRxiv preprint doi: https://doi.org/10.1101/2022.05.15.491997; this version posted May 15, 2022. The copyright holder for this preprint (which was not certified by peer review) is the author/funder, who has granted bioRxiv a license to display the preprint in perpetuity. It is made available under aCC-BY-NC 4.0 International license.

values corresponding to the frequency bins within each frequency band ($\theta = 4 - 8Hz, \alpha = 8 - 13Hz, \beta = 13 - 30Hz$). We also obtained the Weighted Node Degree (or Node Strength) for a given ROI by summing the $\underline{\Gamma}$ values of all its connections. In the context of graph theory, Weighted Node Degree is one of the simplest and the most intuitive local network measures to evaluate the contribution of a given node (or an ROI) to the connectivity network.

2.6 Mean-centered Partial Least Squares Correlation (MC-PLSC)

Partial Least Squares Correlation (PLSC) for neuroimaging applications was introduced by McIntosh [24]. PLSC algorithm is a multivariate technique that is used to explore the statistical association between two sets of variables. Depending on the research question, we can choose one of the variants of PLSC such as behavior PLSC (brain- and behavior measures as two different variables), task PLSC (brain measures corresponding to two different conditions/tasks such as attention vs. rest), or seed PLSC (to analyze the functional connectivity in a particular 'seed' or a brain region of interest) [25]. PLS algorithm has an inherent advantage of dealing with more variables (P) than the number of observations (or samples N) which is suitable for most neuroimaging studies. In this study, we used the Mean-Centered task PLSC (called MC-PLSC henceforth), which is conceptually very similar to Barycentric Discriminant Analysis (BADA) [26] in the sense MC-PLSC allows us to find sets of features (brain measures) that best maximize the absolute differences between the groups. In MC-PLSC, group labels are used as the dummy coded categorical variables (instead of the continuous behavioral measure in the case of Behavioral PLSC). To know more about the intricacies of different forms of PLSC, we recommend a review article by [25].

To briefly explain the procedure of mean-centered PLSC, one can consider the brain measure matrix $\mathbf{X} \in \mathbb{R}^{N \times P}$ and the dummy coded matrix $\mathbf{Y} \in \mathbb{R}^{N \times m}$, where 'm' - the number of columns corresponds to the number of groups. Here, the number of columns in $\mathbf{X}$ (i.e. P) corresponds to the number of features derived from the brain imaging (e.g. functional connectivity/structural connectivity/power-spectrum density values, etc.). The number of rows in both $\mathbf{X}$ and $\mathbf{Y}$ corresponds to the number of subjects N. In this study, we used the weighted node degree values corresponding to 20 ROIs as our brain imaging variables, and also in secondary analysis, we used the functional connectivity values between 20 ROIs (a vector of ${}^{20}C_2 = 190$ connections per subject) as brain imaging variables. After standardizing the $\mathbf{X}$ using z-score normalization, we define a matrix M such that $\mathbf{M} = \text{diag}(\mathbf{1^T Y})^{-\mathbf{1}}\mathbf{Y^T X}$, where $\mathbf{1}$ is a $N \times 1$ vector of 1s. This matrix scales the X according to the mass of $\mathbf{X}$ (the values are scaled such that the sum of the masses is equal to one). Thereafter, the mean-centered matrix is computed as $\mathbf{R}_{mean-centered} = \mathbf{M} - \mathbf{1}[\frac{1}{N}\mathbf{1}^T\mathbf{M}]$, where $\mathbf{1}$ is a N-length vector of 1s [25].

$\mathbf{R}$ is then subjected to the singular value decomposition as $\mathbf{R} = \mathbf{U\Delta V}^\top$where $\mathbf{U}$ and $\mathbf{V}$ are matrices composed of left and right singular column vectors ($\mathbf{u}_k$ and $\mathbf{v}_k$) and $\mathbf{\Delta}$ a diagonal matrix of singular values (δ_k), k being the number of latent variables corresponding to the number of groups (k =3 in our study). In the context of our PLSC study, $\mathbf{U}$ and $\mathbf{V}$ are termed design/group salience and brain salience reflecting the group contrast and weighted contribution by the brain functional connectivity features respectively. Furthermore, the projection of $\mathbf{Y}$ and $\mathbf{X}$ onto these salience matrices ($\mathbf{U}$and $\mathbf{V}$) reflects the design scores (i.e. $\mathbf{L}_Y = \mathbf{YU}$) and brain scores ($\mathbf{L}_X = \mathbf{XV}$) respectively. The mean-centered PLSC effectively decomposes $\mathbf{R}$ into $k$components that optimally separate the groups by finding pairs of group/design and brain latent vectors with maximal covariance.

To assess the statistical significance of the PLSC models, we ran non-parametric permutation testing, wherein, each latent variable (LV) is tested for its significance. In this procedure, the brain imaging features are randomly shuffled 1000 times and the latent variables are computed using PLSC every time. This way, the original relationship between brain imaging ($\mathbf{X}$) and group label data ($\mathbf{Y}$) is no longer valid. The latent variable k is considered significant if the empirical singular value (δ_k) is higher than 95% of the values obtained from the null distribution. Provided the latent variable is significant, we tested which of the loading weights ($\mathbf{v}_{k,i}$) are robust/stable amongst the brain connectivity features. For this, we conducted a bootstrap procedure wherein, the rows of the $\mathbf{X}$ and $\mathbf{Y}$ were sampled with replacement. Since the permutation and

bioRxiv preprint doi: https://doi.org/10.1101/2022.05.15.491997; this version posted May 15, 2022. The copyright holder for this preprint (which was not certified by peer review) is the author/funder, who has granted bioRxiv a license to display the preprint in perpetuity. It is made available under aCC-BY-NC 4.0 International license.

bootstrapping procedure can affect the alignment(rotation) of the LVs, we applied Procrustes rotation to these LVs so that they correspond to the original data [27].

Confidence Intervals: To test whether the separation between groups was significant, we used generalized Principal Component Analysis to project the factor scores [26]. The factor scores were obtained as the product of the left singular vector and singular values, i.e., $F = \mathbf{U}\mathbf{\Delta}$. These factor scores were then projected onto a 2-dimensional map. 95% confidence interval of these factor scores was obtained using bootstrapped sampling, where the factor scores were obtained for every sampling. Fig. 3(c) and Fig. 4(c) shows the 95% confidence ellipses for each group on the 2-dimensional map.

3 Results

3.1 Univariate Analysis of Behavioral Measures

This study compared the behavioral measures based on COP displacement during High backward perturbation and Berg Balance Scale (BBS). While the COP displacement measures the ability to dynamically maintain balance in response to balance perturbation, BBS is a measure of static and dynamic functional balance and thus provides complementary information [28]. A univariate analysis based on a two-tailed t-test revealed that the TBI patients (mean $\pm$ SD = 11.64 $\pm$ 4.28, 95% CI =[4.79, 19.18]) showed significantly larger COP displacement (t = 3.07, p = 0.004, cohen's D = 1.09) than HC(mean $\pm$ SD = 7.82 $\pm$ 2.33, 95% CI = [4.7, 13.13]). These results are previously presented in [29]. In this study, we further looked into the stratified analysis of COP displacement (shown in Fig. 2) by comparing the balance-impaired TBI (BI-TBI) and balance nonimpaired TBI (BN-TBI). The difference in COP displacement between BI-TBI (13.04 $\pm$ 4.34) and BN-TBI (10.41 $\pm$ 4.1) was not significant as revealed by the two-tailed t-test (t = 1.28, p = 0.22). The BBS comparison showed a significant difference (t = 5.7, p = 10e-5) between BI-TBI (mean $\pm$ SD = 44.37 $\pm$ 4.84) and BN-TBI (mean $\pm$ SD = 54.22 $\pm$ 1.72). Since the BBS data in HC was non-normal, we used the nonparametric Wilcoxon Ranksum test to compare the BBS in HC (median = 56, range =[55,56]) with that of BI-TBI and BN-TBI. As expected, when compared to HC, both BI-TBI and BN-TBI showed a significantly lower BBS (z = 4.15, p = 10e-5 and z = 4.15 and p = 0.0023 respectively).

bioRxiv preprint doi: https://doi.org/10.1101/2022.05.15.491997; this version posted May 15, 2022. The copyright holder for this preprint (which was not certified by peer review) is the author/funder, who has granted bioRxiv a license to display the preprint in perpetuity. It is made available under aCC-BY-NC 4.0 International license.

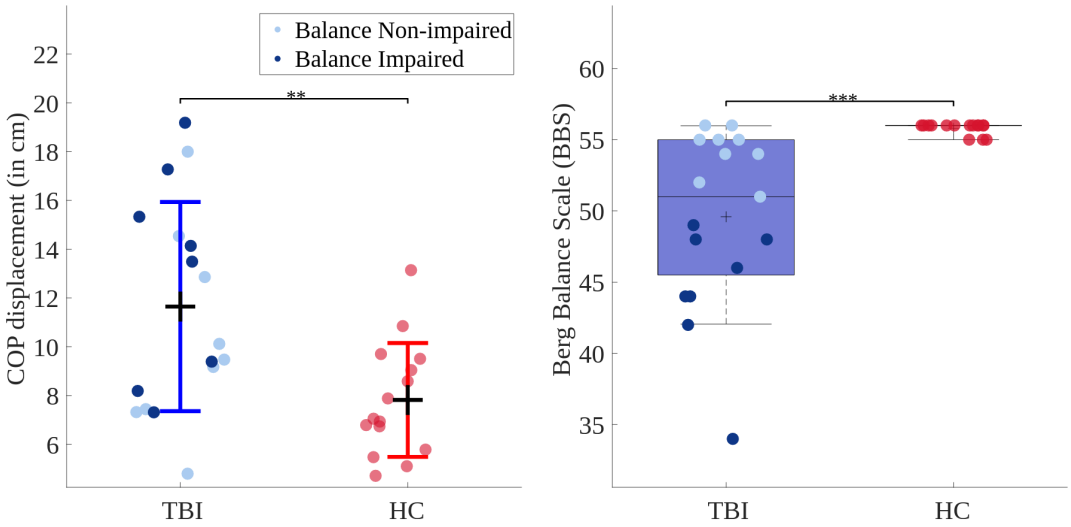

Figure 2: A group-level comparison of COP displacement (in cm) shown on the left. The black horizontal line on the COP plot marks the mean and the colored horizontal line marks the standard deviation. A group-level comparison of the Berg Balance Scale (BBS) is shown on the right as a boxplot due to its non-normal distribution. The horizontal line marks the median. The lower- and upper-hinge of the boxplot corresponds to the 25th and 75th quartile respectively. Statistical significance values are plotted as ***(p<0.005), **(p<0.01) respectively.

bioRxiv preprint doi: https://doi.org/10.1101/2022.05.15.491997; this version posted May 15, 2022. The copyright holder for this preprint (which was not certified by peer review) is the author/funder, who has granted bioRxiv a license to display the preprint in perpetuity. It is made available under aCC-BY-NC 4.0 International license.

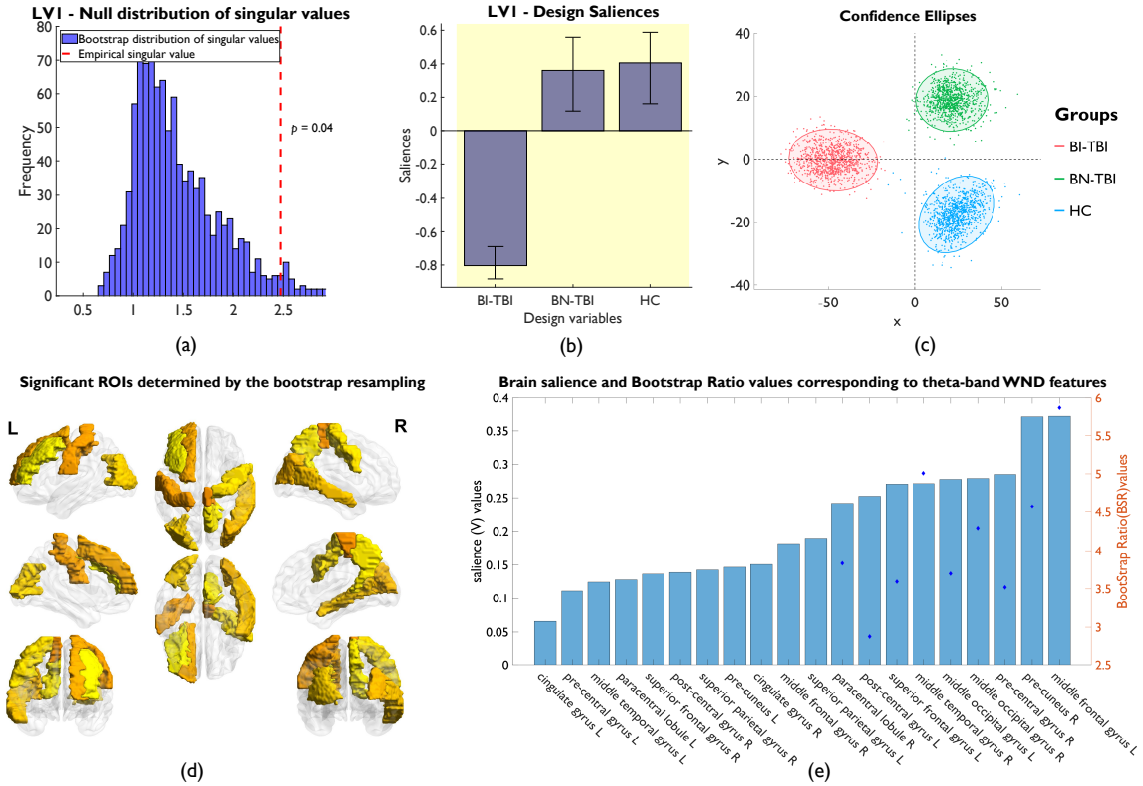

Figure 3: (a) Histogram of the singular values obtained from the first latent variable (LV1) corresponding to mean-centered PLSC. The latent variable denotes the contrast BI-TBI vs. (HC and BN-TBI). The brain imaging variable here is Theta-band weighted node degree and the design variable is the group label. The singular value obtained from the PLSC is tested for its significance using the permutation test. The red dotted line denotes the empirical singular value (statistically significant- above 95th percentile of the singular values obtained from null distribution), and the blue bar graph presents the histogram of values obtained under null distribution. (b) Design saliences ($\mathbf{u}_1$ vector after SVD) indicate that the BI-TBI group is significantly different from BN-TBI and HC, with the error bars indicating the 95% confidence interval. The yellow background indicates robust salience values for all 3 groups. (c) 95% confidence ellipses denote a clear separation of BI-TBI from BN-TBI and HC the first latent group/contrast vector (x-direction) associated with LV1 but not so for the second latent vector (y-direction) associated with LV2 (p=0.93). (d) Highlighted brain regions of interest for LV1 correspond to the robust variables selected based on the bootstrapping ratio (BSR) and (e) the bar graph values indicate the brain saliences ($\mathbf{v}_1$ vector) associated with LV1 obtained from bootstrapping. The robust ROIs (Bootstrap ratio>2.5); the robust region and bootstrap values are denoted with a blue diamond mark.

bioRxiv preprint doi: https://doi.org/10.1101/2022.05.15.491997; this version posted May 15, 2022. The copyright holder for this preprint (which was not certified by peer review) is the author/funder, who has granted bioRxiv a license to display the preprint in perpetuity. It is made available under aCC-BY-NC 4.0 International license.

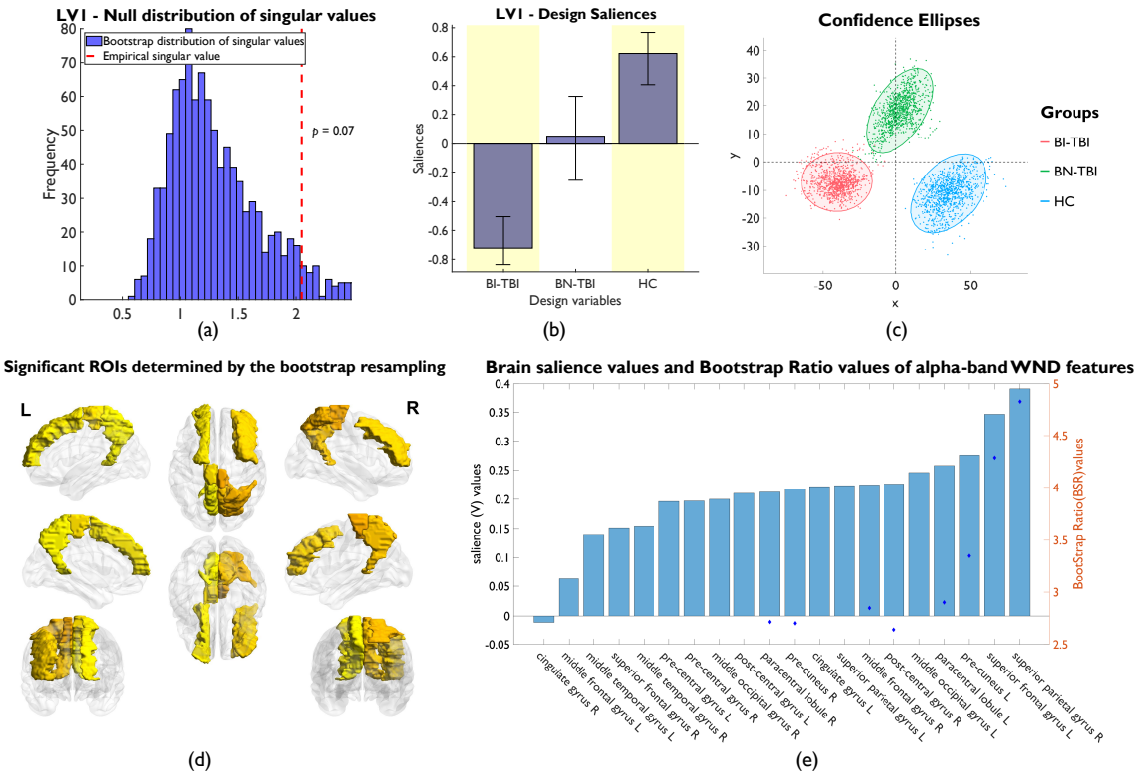

Figure 4: (a) Histogram of the singular values obtained from the first latent variable (LV1) corresponding to the contrast BI-TBI vs. (BN-TBI and HC). The brain imaging variable here is alpha-band weighted node degree and the design variable is the categorical label (mild-impaired TBI as 1, severe-impaired TBI as -1). The singular value obtained from the PLSC is tested for its significance using the permutation test. The red dotted line denotes the empirical singular value (statistically significant- above 95th percentile of the singular values obtained from null distribution), and the blue bar graph presents the histogram of values obtained under null distribution. (b) Design saliences ($\mathbf{u}_1$) indicate that the BI-TBI group is significantly different from HC with the error bars indicating the 95% confidence interval of bootstrapped saliences. The yellow background indicates robust salience values for BI-TBI and HC groups but not BN-TBI. (c) Confidence ellipses clearly denote the separation between HC and BI-TBI along the dimension-1 (x-axis) associated with LV1, but not BN-TBI as its confidence ellipse is spanning both negative and positive x-values. Also, confidence ellipses for LV2 (y-axis) overlap highlight the lack of significant group separation (p=0.99) (d) Highlighted brain regions of interest correspond to the robust variables selected based on the bootstrapping ratio (BSR) for LV1 and (e) the bar graph values indicate the brain saliences contribution ($\mathbf{v}_1$ vector) associated with LV1 obtained from bootstrapping. The robustness of each variable is determined based on the ratio (>2.5); the robust regions and bootstrap values are highlighted with a blue diamond mark.

3.2 Mean-centered PLSC: Weighted Node Degree features

Upon dichotomizing the TBI group into BI-TBI and BN-TBI based on the BBS threshold, we ran mean-centered PLSC with 3 groups (BI-TBI, BN-TBI, and HC) as design variables, and weighted node degree features as the brain imaging variables. We suspected that the level of balance impairment would also play a role in identifying the discriminative neural markers. Based on this analysis framework, we observed that

bioRxiv preprint doi: https://doi.org/10.1101/2022.05.15.491997; this version posted May 15, 2022. The copyright holder for this preprint (which was not certified by peer review) is the author/funder, who has granted bioRxiv a license to display the preprint in perpetuity. It is made available under aCC-BY-NC 4.0 International license.

the MC-PLSC using weighted node degree (WND) features in theta frequency band identified LV1 as a significant latent variable (out of three) that maximally differentiates the groups by contrasting BI-TBI from BN-TBI and HC together (Fig. 3(b)). The nonparametric permutation testing revealed that the empirical singular value is in the top 5 percentile of the permutated singular values (Fig. 3(a)), thus highlighting the statistical significance (p = 0.039) of LV1. Upon bootstrap testing of this LV, 9 ROIs were found to be robustly associated with LV1 having their Bootstrap Ratio (BSR) > 2.5 (Fig. 3(e)) i.e., their salience values/weighted contributions were found to be non-zero with a 99% confidence interval. The robust WND features are presented in (Fig. 3(d & e)), the regions highlighted (in the descending order of their salience values) are - left middle frontal gyrus, right precuneus, right precentral gyrus, bilateral middle occipital gyrus, right middle temporal gyrus, left superior frontal gyrus, left post-central gyrus, right paracentral lobule.

In a post-hoc analysis of individual group-wise contrast PLSC (i.e., one group contrast at a time - BI-TBI vs. BN-TBI, and BI-TBI vs. HC) using theta-band WND features, we noticed that the robust ROIs were, in fact, the same set of cortical regions found in the above MC-PLSC analysis (BI-TBI distinguishing BN-TBI and HC). This supports the notion that the neural substrates of balance impairment for BI-TBI could be the very same ROIs when compared to both BN-TBI and HC.

A similar analysis using the alpha-band WND features revealed LV1 to be significantly distinguishing BI-TBI from BN-TBI and HC (Fig. 4(b) and Fig. 4(c)). LV1 was associated with a slightly different set of robust regions based on the bootstrap ratio: left superior frontal gyrus, right postcentral gyrus, right mid frontal gyrus, right superior parietal lobule, bilateral paracentral lobules, and bilateral precuneus.

3.3 Mean-centered PLSC: Individual Connectivity Features

To further investigate the localized roles of individual functional connections which correlate with the contrast of different groups, we ran the MC-PLSC with the individual connectivity features (connection strength between two regions) derived from imaginary coherence in each frequency band (theta, alpha, and beta). This analysis revealed only theta-band connectivity features to be distinguishing impaired TBI from the rest (BI-TBI different from BN-TBI and HC) with a marginally significant result ($p = 0.069$). The circular connectivity plot is shown in Fig. 5. Significant connections are highlighted based on the bootstrapped ratio (BSR) > 2.6 suggesting that the connections have a 99% confidence level in terms of robustness to spurious connectivity features. Based on the connectivity pattern shown in Fig. 5, we observed that the distinction between the impaired and the non-impaired population (BN-TBI and HC) is reflected by weaker connections (BI-TBI < BN-TBI and HC) involving the left superior parietal lobule, left postcentral gyrus, right mid occipital gyrus, and right paracentral lobule. Most of these robust connections are associated with the sensorimotor network (postcentral gyrus, paracentral lobule, and even middle temporal gyrus) and visual network[30]).

bioRxiv preprint doi: https://doi.org/10.1101/2022.05.15.491997; this version posted May 15, 2022. The copyright holder for this preprint (which was not certified by peer review) is the author/funder, who has granted bioRxiv a license to display the preprint in perpetuity. It is made available under aCC-BY-NC 4.0 International license.

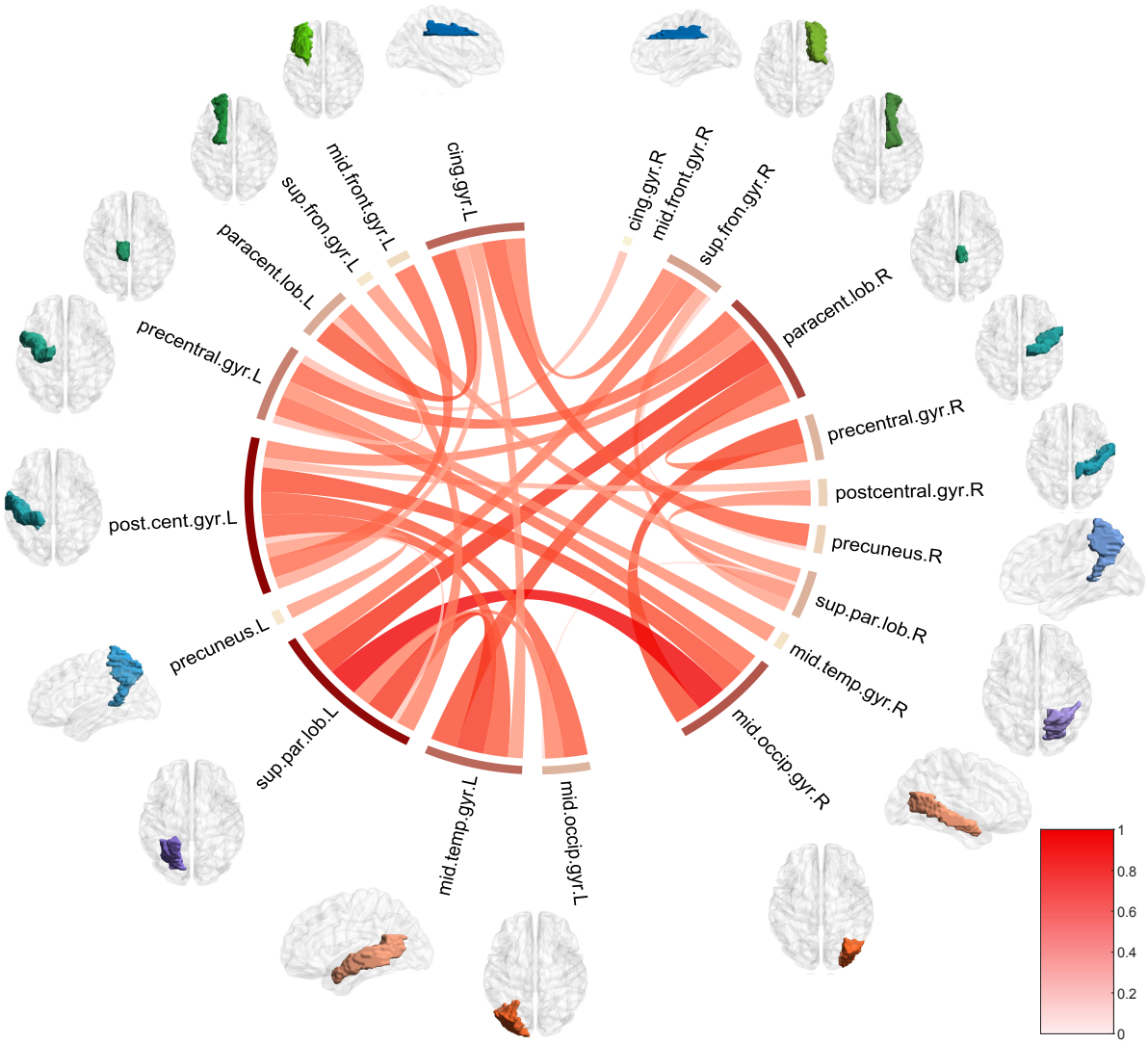

Figure 5: Visualization of robust functional connections derived from theta-band imaginary coherence based on the $|\text{BSR}| > 2.6$. The color of the connectivity links corresponds to the first latent variable of the brain salience matrix ($\mathbf{v}_1$). The thickness of the connectivity value (between two ROIs) indicates its proportional contribution to the weighted node degree of a given ROI (thicker connection - higher proportion, thinner connection - lower proportion). The color of the sector (outer circle) indicates the absolute sum of connectivity values corresponding to a given ROI (darker color shade denotes a higher sum). The cortical ROIs are visually represented as a volumetric ROI next to the label. The circular connectivity graph is visualized using the R package *circlize* [31].

bioRxiv preprint doi: https://doi.org/10.1101/2022.05.15.491997; this version posted May 15, 2022. The copyright holder for this preprint (which was not certified by peer review) is the author/funder, who has granted bioRxiv a license to display the preprint in perpetuity. It is made available under aCC-BY-NC 4.0 International license.

4. Discussion

4.1. Disentangling the levels of balance impairment in TBIs

We noticed that the level of task-specific balance impairment was varied across individuals within the TBI group based on the measure of COP displacement. Although we hypothesized that the body sway during the external perturbation measured by COP displacement would be smaller in the BI-TBI group compared to the BN-TBI group, we did not see any significant differences. We suspect the reason could be that the BBS is strongly correlated with the gross functional outcome measure (such as Timed Up-and-Go) rather than the laboratory measures of body sway (measured using COP displacement). We certainly recommend future studies to investigate the association between the outcome measure specific to the experimental task and the traditional functional outcomes such as BBS and/or Balance Error Scoring System.

Recent literature suggests that balance complaints from chronic TBI individuals are explained more by the dysfunction of central sensory systems than the peripheral vestibular or oculomotor systems [32]. In the following subsections, we discuss the role of different cortical regions and functional networks in the postural control mechanisms in TBI.

4.2. Main PLSC findings

Our MC-PLSC analysis found a WND latent vector of brain regions that robustly and maximally separate the 3 groups (BI-TBI, BN-TBI, and HC) for theta and marginally so for the alpha band. The associated contrast vector for theta (Fig. 3(b)) reveals that the groups are maximally separated when contrasting BI-TBI with BN-TBI and healthy controls combined. This suggests that the theta neural response for BN-TBI is more like that of HC. But more importantly, BI-TBI individuals do present an impaired neural response (decrease in WND) to the balance perturbation, which is specific to balance impairment as measured by the BBS. This observation supports our hypothesis and rationale for separating TBIs into balance-impaired and non-impaired populations. Furthermore, this could potentially explain why in our prior analysis [33], no group difference in a global measure of WND connectivity was found when contrasting HC with both BI- and BN-TBIs combined.

In comparison, for alpha (Fig. 4(b)) the groups are maximally separated when only contrasting BI-TBI and HC alone, excluding BN-TBI. This would suggest that BN-TBI doesn't separate well from either BI-TBI or HC. Furthermore, based on the brain and contrast saliences of this latent variable, BN-TBI shows reduced alpha WND compared to HC. However, given that BI-TBI and HC are defined both by BBS score but also the overall TBI pathology, this latent variable characterized by a reduced alpha WND in TBI may not be a specific marker of balance deficit. This is supported by the fact that no significant latent variable was found when running a post-hoc PLSC analysis between BI-TBI and BN-TBI (p=0.48; results not shown) which are solely differentiated by their BBS impairment score.

Finally, similar to theta WND, our contrast analysis on individual connectivities reveals a close to a significant latent variable (p=0.07) that best differentiates groups when contrasting BI-TBI from both BN-TBI and HC. Similarly, based on the corresponding brain and contrast salience values, BI-TBI shows reduced theta connectivities compared to HC and BN-TBI. The overall finding of theta band disconnectivity as a specific marker of balance deficit in TBI is consistent with its critical role in postural control [34]

4.3. Balance-related cortical regions of interest and connectivity identified by PLSC:

The current study found that the main ROIs identified by MC-PLSC across theta- and alpha-band coherence WND features are the right paracentral lobule and precuneus, and the left superior frontal gyrus. These

bioRxiv preprint doi: https://doi.org/10.1101/2022.05.15.491997; this version posted May 15, 2022. The copyright holder for this preprint (which was not certified by peer review) is the author/funder, who has granted bioRxiv a license to display the preprint in perpetuity. It is made available under aCC-BY-NC 4.0 International license.

cortical regions are associated with the sensorimotor coordination required for postural control. Specifically, the paracentral lobule processes the motor commands for balance control [35] after receiving the sensory inputs from the visual, vestibular, and somatosensory cortices. In the context of theta-band functional connectivity, the supplementary motor area located just in front of the paracentral lobule is associated with the pull perturbation while standing [34].

Extending further, the entire closed-loop mechanism of balance control as coordination between several brain regions is described as the '*body schema*' in the hypothetical model [36]. As per this model of posture-gait control, the midbrain and subcortical regions including the cerebellum, brainstem, thalamus, and cerebral cortex receive the sensory signals from the visual cortex, vestibular cortex, and primary sensory cortex, which will then be processed by the temporoparietal cortex to construct the aforementioned *body schema.* Specifically, the temporoparietal cortex assists in generating motor control commands from the supplementary motor area (SMA) and premotor (PM) regions, with the help of basal ganglia and cerebellum. In our study, the middle frontal gyri which include the SMA/PM region seem to play a distinctive role in the BI-TBI group (when compared to BN-TBI and HC) as revealed by its robust bootstrap ratio in the MC-PLSC model derived from theta-band WND features. From a functional perspective, the role of middle frontal gyri in anticipated postural control is highlighted in [37]. Moreover, the middle frontal gyri are reported to be involved in the supraspinal motor network of stance and locomotion of walking in elderly adults [38].

Once the sensory signals are received and processed by visual, vestibular, and somatosensory cortices, the motor commands for balance control are processed by the paracentral lobule and precentral gyrus [39] which constitutes the leg region of the M1. In the framework of the posture-gait control model mentioned in [36], we believe that the superior parietal region is involved in anticipatory postural adjustment as it detects postural instability [40]. Along the same line of discussion, our findings of theta-band coherence-based individual connectivity features show that significant functional connections are associated with the left superior parietal lobule in addition to the right paracentral lobule and left postcentral gyrus. Based on the role of the cingulate and angular gyrus in the dynamic regulation of attention to unpredictable events presented in [41], and their anatomical relation with the basal ganglia and cerebellum, we expect that the postural control signals generated by the motor regions are passed to the cortico-reticular and reticulospinal tracts via cingulate gyrus.

In terms of the visual perception of the balance perturbation, we anticipate the regions around the occipital lobe will play an integral role in the visual perception of static vs. dynamic motion (or tilt) of the posturography platform based on the report of an Activation Likelihood Estimation (ALE) meta-analysis article [42]. Along this line of discussion, we believe the middle occipital gyrus identified by the theta-band WND features in our study may play a critical role in the sensory integration of visual and motor functions [43]. Moreover, the activation of middle temporal gyri has been reported in the simulation (or imagination) of a postural control study [44,45], wherein the activated areas were shown to be in close proximity to the PIVC (parietal insular vestibular cortex) - a region that is generally regarded as responsible for processing the vestibular signals related to the postural control [36].

4.4. Roles of different functional networks identified by PLSC

For qualitative assessment of our findings, we now discuss the roles of functional networks to which the aforementioned ROIs belong.

Although it is not trivial to assign the anatomical ROIs to specific functional networks, a recent study has tested the spatial correspondence between the anatomical regions (based on the Desikan-Killiany atlas) and functional networks (based on the Yeo-Atlas) [46]. The permutation testing of the normalized mutual information showed that the hypothesized overlap between the functional networks and anatomical ROIs was not due to random chance. In other words, the nonparametric testing supported the evidence that the functional networks and anatomical ROIs have good spatial correspondence. Motivated by this idea, we wanted to explore the role of the significant ROIs returned by the PLSC analysis in the context of functional

bioRxiv preprint doi: https://doi.org/10.1101/2022.05.15.491997; this version posted May 15, 2022. The copyright holder for this preprint (which was not certified by peer review) is the author/funder, who has granted bioRxiv a license to display the preprint in perpetuity. It is made available under aCC-BY-NC 4.0 International license.

networks involved in postural control. In this regard, our focus is mainly on the two intrinsic functional networks: the sensorimotor network (SMN) and the visual network (VN), as these networks showed high spatial correspondence with the motor and visual areas as per the Desikan Killiany Atlas[46]. Not surprisingly, the sensorimotor network (SMN) is reported to play the most critical role during postural control mechanisms by facilitating sensorimotor integration [47]. While the roles of different regions within the SMN are widely studied in the context of postural control [48,39,37], the network-level mechanisms are not well studied in the TBI population. Our study shows preliminary evidence that the functional connectivity network strength of the SMN comprising bilateral paracentral lobule is associated with distinguishing the balance-impaired TBI from balance non-impaired TBI and healthy controls. We also noticed the strongest connectivity feature associated with the Middle Occipital Gyrus (MOG) and the left superior parietal lobule (SPL) (Fig. 5). This finding corroborates those of [49] focused on the neuroimaging of normal and precision gait, where, it was shown that the precise spatial control of the gait depends on the functional interactions between the MOG (part of the visual network) and SPL [30]). Also, the connectivity between MOG and SPL is expected to be involved in the visuospatial perception [50]. With regard to the functional networks, SPL is considered a core region of the *dorsal attention network* (DAN), which is generally preactivated during the anticipatory movement which will subsequently predict performance to upcoming targets. Also, under certain conditions, the preparatory activation of the DAN will extend to the visual cortex reflecting the top-down mechanism of sensory control.

4.5. Limitations

We acknowledge there are several limitations of our study. First, our sample size is relatively small for stratified analysis. Based on our observations, we suggest the future study design of postural control tasks in TBI must take into account the level of impairment (e.g. Berg Balance Scale or Balance Error Scoring System) and not just the level of severity (mild/moderate/severe) based on Glasgow Coma Scale at the time of injury. Moreover, we did not study the task-specific activity of deep sub-cortical neural substrates such as the brainstem, basal ganglia, and pedunculopontine nucleus which are involved in the postural control [35] given the limited accuracy of EEG source localization of subcortical structures.

Conclusion

In this study, we present for the first time, a stratified analysis of balance deficits in TBI by studying the brain connectivity features pertaining to the balance perturbation task. As the heterogeneity in TBI poses the challenge in identifying robust brain imaging features correlated with the impairment, we used a multivariate statistical framework based on the partial least squares correlation. We made several interesting observations including, (1) COP displacement - an outcome measure of balance control did not seem to distinguish the balance-impaired TBI from non-impaired TBI as we observed in the case of BBS; (2) The MC-PLSC algorithm with the theta-band functional connectivity network strength of selected anatomical regions as the brain imaging features showed specific ROIs that distinguished BI-TBI from BN-TBIs and HC. These selected regions namely- paracentral lobules, precuneus, superior parietal lobule, superior frontal gyrus play a critical role in postural control; (3) The MC-PLSC algorithm with individual functional connectivity values as imaging features revealed that the weaker functional connections in BI-TBI (compared to BN-TBI and HC) linked to the leg motor region (paracentral lobule) may be indicative of maladaptive balance performance. Understanding the role of key regions of interest may help in designing novel therapeutic interventions (e.g., neuromodulation and/or goal-directed movement therapies) for improving the balance functions in TBI.

bioRxiv preprint doi: https://doi.org/10.1101/2022.05.15.491997; this version posted May 15, 2022. The copyright holder for this preprint (which was not certified by peer review) is the author/funder, who has granted bioRxiv a license to display the preprint in perpetuity. It is made available under aCC-BY-NC 4.0 International license.

References

1.Thompson, H. J., McCormick, W. C. & Kagan, S. H. Traumatic brain injury in older adults: epidemiology, outcomes, and future implications. *Journal of the American Geriatrics Society* **54**, 1590–1595 (2006).

2.Pickett, T. C. Objectively assessing balance deficits after TBI: Role of computerized posturography. *The Journal of Rehabilitation Research and Development* **44**, 983–990 (2007).

3.Fino, P. C. *et al.*. Assessment and rehabilitation of central sensory impairments for balance in mTBI using auditory biofeedback: a randomized clinical trial. *BMC Neurology* **17**, (2017).

4.Calzolari, E. *et al.*. Vestibular agnosia in traumatic brain injury and its link to imbalance. *Brain* **144**, 128–143 (2020).

5.Wang, B. *et al.*. Posture-related changes in brain functional connectivity as assessed by wavelet phase coherence of NIRS signals in elderly subjects. *Behavioural Brain Research* **312**, 238–245 (2016).

6.Varghese, J. P., Staines, W. R. & McIlroy, W. E. Activity in Functional Cortical Networks Temporally Associated with Postural Instability. *Neuroscience* **401**, 43–58 (2019).

7.Caeyenberghs, K. *et al.*. Brain connectivity and postural control in young traumatic brain injury patients: A diffusion MRI based network analysis. *NeuroImage: Clinical* **1**, 106–115 (2012).

8.Caeyenberghs, K. *et al.*. Brain-behavior relationships in young traumatic brain injury patients: DTI metrics are highly correlated with postural control. *Human Brain Mapping* **31**, 992–1002 (2009).

9.Han, K., Chapman, S. B. & Krawczyk, D. C. Disrupted Intrinsic Connectivity among Default Dorsal Attention, and Frontoparietal Control Networks in Individuals with Chronic Traumatic Brain Injury. *Journal of the International Neuropsychological Society* **22**, 263–279 (2016).

10.Woytowicz, E. J., Sours, C., Gullapalli, R. P., Rosenberg, J. & Westlake, K. P. Modulation of working memory load distinguishes individuals with and without balance impairments following mild traumatic brain injury. *Brain Injury* **32**, 191–199 (2017).

11.Churchill, N. W., Hutchison, M. G., Graham, S. J. & Schweizer, T. A. Connectomic markers of symptom severity in sport-related concussion: Whole-brain analysis of resting-state fMRI. *NeuroImage: Clinical* **18**, 518–526 (2018).

12.Handiru, V. S. *et al.*. Graph-theoretical Analysis of EEG Functional Connectivity during Balance Perturbation in Traumatic Brain Injury: A Pilot Study. (2020) doi:10.1101/2020.10.08.332353.

13.Stevenson, T. J., Connelly, D. M., Murray, J. M., Huggett, D. & Overend, T. Threshold Berg Balance Scale Scores for Gait-Aid Use in Elderly Subjects: A Secondary Analysis. *Physiotherapy Canada* **62**, 133–140 (2010).

14.Chang, C.-Y., Hsu, S.-H., Pion-Tonachini, L. & Jung, T.-P. Evaluation of Artifact Subspace Reconstruction for Automatic Artifact Components Removal in Multi-Channel EEG Recordings. *IEEE Transactions on Biomedical Engineering* **67**, 1114–1121 (2020).

15.Makeig, S., Bell, A. J., Jung, T.-ping & Sejnowski, T. J. Independent Component Analysis of Electroencephalographic Data. in *Advances in Neural Information Processing Systems 8* (1996).

16.Pion-Tonachini, L., Kreutz-Delgado, K. & Makeig, S. ICLabel: An automated electroencephalographic independent component classifier, dataset, and website.. *Neuroimage* **198**, 181–197 (2019).

17.Handiru, V. S., Vinod, A. P. & Guan, C. EEG Source Imaging of Movement Decoding: The State of the Art and Future Directions. *IEEE Systems Man, and Cybernetics Magazine* **4**, 14–23 (2018).

18.Gramfort, A., Papadopoulo, T., Olivi, E. & Clerc, M. OpenMEEG: opensource software for quasistatic bioelectromagnetics. *BioMedical Engineering OnLine* **9**, 45 (2010).

bioRxiv preprint doi: https://doi.org/10.1101/2022.05.15.491997; this version posted May 15, 2022. The copyright holder for this preprint (which was not certified by peer review) is the author/funder, who has granted bioRxiv a license to display the preprint in perpetuity. It is made available under aCC-BY-NC 4.0 International license.

19.Tadel, F., Baillet, S., Mosher, J. C., Pantazis, D. & Leahy, R. M. Brainstorm: A User-Friendly Application for MEG/EEG Analysis. *Computational Intelligence and Neuroscience* **2011**, 1–13 (2011).

20.Fuchs, M., Drenckhahn, R., Wischmann, H. & Wagner, M. An improved boundary element method for realistic volume-conductor modeling. *IEEE Transactions on Biomedical Engineering* **45**, 980–997 (1998).

21.Pascual-Marqui, R. D. Standardized low-resolution brain electromagnetic tomography (sLORETA): technical details.. *Methods Find Exp Clin Pharmacol* **24 Suppl D**, 5–12 (2002).

22.Shattuck, D. W. & Leahy, R. M. BrainSuite: An automated cortical surface identification tool. *Medical Image Analysis* **6**, 129–142 (2002).

23.Nolte, G. *et al.*. Identifying true brain interaction from EEG data using the imaginary part of coherency. *Clinical Neurophysiology* **115**, 2292–2307 (2004).

24.McIntosh, A. R. & Lobaugh, N. J. Partial least squares analysis of neuroimaging data: Applications and advances. *NeuroImage* **23**, 250–263 (2004).

25.Krishnan, A., Williams, L. J., McIntosh, A. R. & Abdi, H. Partial Least Squares (PLS) methods for neuroimaging: A tutorial and review. *NeuroImage* **56**, 455–475 (2011).

26.Abdi, H. *et al.*. Multiple Subject Barycentric Discriminant Analysis (MUSUBADA): How to Assign Scans to Categories without Using Spatial Normalization. *Computational and Mathematical Methods in Medicine* **2012**, 1–15 (2012).

27.Milan, L. & Whittaker, J. Application of the Parametric Bootstrap to Models that Incorporate a Singular Value Decomposition. *Applied Statistics* **44**, 31 (1995).

28.Berg, K. O., Maki, B. E., Williams, J. I., Holliday, P. J. & Wood-Dauphinee, S. L. Clinical and laboratory measures of postural balance in an elderly population.. *Arch Phys Med Rehabil* **73**, 1073–80 (1992).

29.Shenoy, H. V. *et al.*. Graph-theoretical analysis of EEG functional connectivity during balance perturbation in traumatic brain injury: A pilot study.. *Hum Brain Mapp* **42**, 4427–4447 (2021).

30.Uddin, L. Q., Yeo, B. T. T. & Spreng, R. N. Towards a Universal Taxonomy of Macro-scale Functional Human Brain Networks. *Brain Topography* **32**, 926–942 (2019).

31.Gu, Z., Gu, L., Eils, R., Schlesner, M. & Brors, B. circlize implements and enhances circular visualization in R. *Bioinformatics* **30**, 2811–2812 (2014).

32.Campbell, K. R. *et al.*. Exploring persistent complaints of imbalance after mTBI: Oculomotor peripheral vestibular and central sensory integration function. *Journal of Vestibular Research* 1–12 (2021) doi:10.3233/ves-201590.

33.Shenoy, H. V. *et al.*. Graph-theoretical analysis of EEG functional connectivity during balance perturbation in traumatic brain injury: A pilot study.. *Hum Brain Mapp* **42**, 4427–4447 (2021).

34.Peterson, S. M. & Ferris, D. P. Group-level cortical and muscular connectivity during perturbations to walking and standing balance. *NeuroImage* **198**, 93–103 (2019).

35.Boisgontier, M. P. *et al.*. Individual differences in brainstem and basal ganglia structure predict postural control and balance loss in young and older adults. *Neurobiology of Aging* **50**, 47–59 (2017).

36.Takakusaki, K. Functional Neuroanatomy for Posture and Gait Control. *Journal of Movement Disorders* **10**, 1–17 (2017).

37.Mihara, M., Miyai, I., Hatakenaka, M., Kubota, K. & Sakoda, S. Role of the prefrontal cortex in human balance control. *NeuroImage* **43**, 329–336 (2008).

38.Zwergal, A. *et al.*. Aging of human supraspinal locomotor and postural control in fMRI. *Neurobiology of Aging* **33**, 1073–1084 (2012).

bioRxiv preprint doi: https://doi.org/10.1101/2022.05.15.491997; this version posted May 15, 2022. The copyright holder for this preprint (which was not certified by peer review) is the author/funder, who has granted bioRxiv a license to display the preprint in perpetuity. It is made available under aCC-BY-NC 4.0 International license.

39.Taubert, M., Mehnert, J., Pleger, B. & Villringer, A. Rapid and specific gray matter changes in M1 induced by balance training. *NeuroImage* **133**, 399–407 (2016).

40.Slobounov, S., Wu, T. & Hallett, M. Neural basis subserving the detection of postural instability: an fMRI study.. *Motor Control* **10**, 69–89 (2006).

41.Hahn, B., Ross, T. J. & Stein, E. A. Cingulate Activation Increases Dynamically with Response Speed under Stimulus Unpredictability. *Cerebral Cortex* **17**, 1664–1671 (2006).

42.Dijkstra, B. W. *et al.*. Functional neuroimaging of human postural control: A systematic review with meta-analysis. *Neuroscience & Biobehavioral Reviews* **115**, 351–362 (2020).

43.MacKinnon, C. D. Sensorimotor anatomy of gait balance, and falls. in *Handbook of Clinical Neurology* 3–26 (Elsevier, 2018). doi:10.1016/b978-0-444-63916-5.00001-x.

44.Jahn, K. *et al.*. Brain activation patterns during imagined stance and locomotion in functional magnetic resonance imaging. *NeuroImage* **22**, 1722–1731 (2004).

45.Karim, H. T. *et al.*. Functional MR imaging of a simulated balance task. *Brain Research* **1555**, 20–27 (2014).

46.Alexander-Bloch, A. F. *et al.*. On testing for spatial correspondence between maps of human brain structure and function. *NeuroImage* **178**, 540–551 (2018).

47.Peterka, R. J. & Loughlin, P. J. Dynamic Regulation of Sensorimotor Integration in Human Postural Control. *Journal of Neurophysiology* **91**, 410–423 (2004).

48.Goble, D. J. *et al.*. Brain Activity during Ankle Proprioceptive Stimulation Predicts Balance Performance in Young and Older Adults. *Journal of Neuroscience* **31**, 16344–16352 (2011).

49.Bakker, M. *et al.*. Cerebral correlates of motor imagery of normal and precision gait. *NeuroImage* **41**, 998–1010 (2008).

50.Johns, P. *Functional neuroanatomy. Clinical Neuroscience* 27–47 (Elsevier, 2014). doi:10.1016/b978-0-443-10321-6.00003-5.